

Hot spots in the neutrino flux created by cosmic rays from Cygnus and Vela?

M. Bouyahiaoui^{1*}, M. Kachelrieß², and D. V. Semikoz^{1,3,4}

¹*APC, Université Paris Diderot, CNRS/IN2P3, CEA/IRFU,
Observatoire de Paris, Sorbonne Paris Cité, 119 75205 Paris, France*

²*Institutt for fysikk, NTNU, Trondheim, Norway*

³*INR RAS, 60th October Anniversary prospect 7a, Moscow, Russia and*

⁴*National Research Nuclear University MEPhI, Kashirskoe highway 31, 115409 Moscow, Russia*

An analysis of 7.5 years of data in the high-energy starting event sample has been recently published by the IceCube collaboration. The hottest spot in a search for neutrino sources was found far above the Galactic plane and is thus, at first sight, difficult to reconcile with a Galactic origin. In this work, we calculate the cosmic ray (CR) density around nearby, young supernova remnants assuming anisotropic diffusion. Combining the obtained CR densities with the matter distribution deduced from extinction maps, we find two prominent hot spots: The one close to the most significant point in the IceCube search for point sources is created by CRs from the Cygnus loop and has an intensity corresponding to two to four neutrino events. Another, more extended one may be caused by CRs from Vela if CR trajectories are sufficiently disturbed by the magnetic field in the shell around the superbubble Loop I.

I. INTRODUCTION

Neutrinos are a unique tool to study dense environments and the non-thermal universe [1–3]. High-energy neutrinos may be produced together with photons in hadronic interactions of cosmic rays (CR) close to their sources or during propagation. Since they travel undisturbed, being neither absorbed as high-energy photons nor deflected in magnetic fields as charged particles, they are an ideal tracer of sites where the product of CR and target density is high. Such places can be either the CR sources themselves or dense gas clouds close to the sources. Therefore high-energy neutrino observatories have the potential to identify the yet unknown sources of CRs—and this capability has been one of the key motivation for their construction.

The currently largest of these high-energy neutrino telescopes, the IceCube observatory, has succeeded to establish the existence of a surprisingly large flux of extraterrestrial high-energy neutrinos [4]. In Ref. [5], the IceCube collaboration has reanalyzed 7.5 years of data using neutrinos which interaction vertices are contained inside the fiducial volume of the detector. The energy spectrum of these “HESE” neutrinos is compatible with an unbroken power law $dN/dE \propto E^{-\alpha}$ with a spectral index of $\alpha = 2.87 \pm_{0.19}^{0.20}$. Such a steep spectrum challenges most extragalactic source models. In particular, it requires the production of neutrinos in hidden extragalactic sources, since otherwise the accompanying photons would overshoot the bounds on the diffuse background of extragalactic gamma-rays [6, 7].

A guaranteed contribution to the astrophysical neutrino flux are secondary neutrinos produced in interactions of Galactic “sea” CRs with gas [8, 9]. However, the

magnitude of this flux is, even using optimistic parameters, well below the one observed [10, 11]. Moreover, the arrival directions of the astrophysical neutrinos show not the correlation with the Galactic plane expected in this scenario. Therefore, several alternatives which predict a close to isotropic Galactic neutrino flux were suggested: Such neutrinos may originate from a large Galactic halo, formed either by CRs [12, 13] or heavy dark matter particles [14–16], or from the Fermi bubbles [17, 18]. Alternatively, a significant contribution to the Galactic neutrino flux may be rather local, produced by CR interactions at the boundary the Local Bubble (LB) [19, 20].

Studies of specific Galactic neutrino sources have mostly been based on the gamma-ray–neutrino connection: Since the production spectra of gamma-rays and neutrinos in hadronic interactions are correlated, estimates and strict upper bounds on the neutrino flux can be deduced from gamma-ray observations for specific CR sources, see e.g. Ref. [21]. In the case of young CR sources, the finite, energy-dependent distance CRs diffuse may lead, however, to a low-energy cutoff in the secondary spectrum. Therefore gamma-ray observations which are typically limited to energies $\mathcal{O}(\text{TeV})$ restrict only weakly the neutrino flux from such sources at $\mathcal{O}(100 \text{ TeV})$. As result, the brightest spots in the Galactic neutrino sky may be gas clouds immersed into the CR overdensities close—but not close enough to be visible in TeV gamma-rays—to nearby young CR sources [10].

In this work, which is an extension and update of Ref. [22], we study if the nearest Galactic CR accelerators may be visible as neutrino sources. We calculate the CR density around nearby, young supernova remnants (SNR), assuming anisotropic diffusion as suggested in Refs. [23–25]. The faster diffusion of CRs along magnetic field lines implies that gas clouds can give an important contribution to the secondary neutrino flux at larger distances than in the case of isotropic diffusion, if their perpendicular distance to the magnetic field line through the CR source is small. In addition, the slow diffusion per-

*Now at Max-Planck-Institut für Kernphysik, Heidelberg, Germany

pendicular to the magnetic field enhances the CR density close to magnetic field lines connected to the CR sources. We extract the local matter distribution acting as target for neutrino production from extinction maps derived in Refs. [26, 27]. Combining then this matter map with the calculated CR densities, we find two prominent hot spots: The one close to the most significant point in the IceCube search for point sources is created by CRs from the Cygnus Loop supernova remnant (SNR). We estimate the neutrino intensity of this hot spot and find it compatible with two to four events observed by IceCube with energy above 60 TeV. The other one, produced by CRs from the Vela SNR, is at first sight absent in the IceCube HESE sample. However, the CR flux from Vela should be spread out by the enhanced magnetic field in the wall around the superbubble Loop I. We point out that the region around the intersection of Loop I with the peak of the predicted CR intensity has an excess of observed neutrino events, supporting this interpretation.

II. LOCAL COSMIC RAY SOURCES

We choose to use as potential CR sources SNRs which are younger than 30 kyr and located closer than 1 kpc from the Sun. Table I summarizes the available information¹ on these sources. For the calculation of the CR density around these SNRs, we use the same approach as in Refs. [20, 28]: We calculate the trajectory of individual CRs using the Lorentz equation, and find the CR density from the time spent by CRs in space cells. We approximate the Galactic magnetic field by the Jansson-Farrar model [29, 30], with a reduced turbulent field as suggested in Refs. [23–25]. Turbulent magnetic fields are generated using nested grids as described in [31, 32] which allows us to include a large dynamic range of spatial scales contributing to the turbulence. The turbulent magnetic field is taken to be randomly directed with modes distributed between $L_{\min} = 1$ AU and $L_{\max} = 25$ pc according to an isotropic Kolmogorov power spectrum.

Moreover, we modify this model as described in Ref. [20] to take into account the Local Bubble. We apply an exponential damping of the magnetic field inside the bubble as function of the distance z to the Galactic plane with height scale $z_b = 100$ pc. We assume that the strength of the regular magnetic field inside the bubble depends only on the radius r and z , setting $B_{\text{in}} = 0.1\mu G$ inside the bubble and $B_{\text{sh}} = 8 - 12\mu G$ in the wall. Inside the bubble and the wall, we use a clockwise oriented magnetic field for $y > 0$ and an anticlockwise one for $y < 0$. We interpolate the transition between different magnetic field regimes by logistic functions $T(r)$. The width of the two transitions is parameterised by $w_{i=1,2}$,

while w denotes the extension of the wall. We set

$$T_{1/2} = \left[1 + \exp\left(-11 \frac{r - R \pm w/2}{w_{1/2}}\right) \right]^{-1} \quad (1)$$

The Sun is assumed to be at the centre of the LB. In this configuration the turbulent magnetic field strength is set as follows. For $r > R - w/2$: $B_{\text{turb}} = B_{\text{reg}}/2$, and for $r \geq R - w/2$: $B_{\text{turb}} = 5B_{\text{reg}}$, where we use as numerical values $w_1 = 1$ pc, $w_2 = 0.1$ pc, $w = 2$ pc and $R = 100$ pc.

Source	Name	τ /kyr	d /kpc
G065.3+05.7	–	20	0.8
G074.0-08.5	Cygnus Loop	15	0.75
G106.3+02.7	Boomerang	10	0.8
G114.3+00.3	–	7.7	0.7
G160.9+02.6	HB9	5.5	0.8
G263.9-03.3	Vela	11	0.29
G266.2-01.2	Vela Jr	3.8	0.75
G330.0+15.0	Lupus Loop	23	0.33
G347.3-00.5	–	1.6	1
B1737-30	–	20.6	0.4

TABLE I: Cosmic ray sources considered with average values for their age τ and distance d from the Sun.

No detailed model for the time-dependent escape spectrum of accelerated CRs exist. Since we are interested only in CRs with the highest energies which are accelerated before the end of the Taylor-Sedov phase, we can however assume that these CRs escaped at a time much smaller than the age τ of the source. Moreover, we employ the same injection spectrum for all sources for which we choose motivated by the results of Ref. [20] a broken power law in rigidity $\mathcal{R} = E/(Ze)$ with a break at $\mathcal{R}_{\text{br}} = 2 \times 10^{15}$ V and an exponential cut-off at $\mathcal{R}_{\text{max}} = 8 \times 10^{15}$ V,

$$\frac{dN_i}{d\mathcal{R}} = \begin{cases} N_i \mathcal{R}^{-2.2}, & \text{if } \mathcal{R} < \mathcal{R}_{\text{br}} \\ \tilde{N}_i \mathcal{R}^{-3.1} \exp(-\mathcal{R}/\mathcal{R}_{\text{max}}), & \text{if } \mathcal{R} \geq \mathcal{R}_{\text{br}}. \end{cases} \quad (2)$$

We inject 5.000 protons per energy at the position of each source and propagate them for the time τ in our magnetic field model. Then we calculate the CR density $n(E)$ in each cell of size $(6 \text{ pc})^3$. The energy injected in CRs by each source is chosen as 3.5×10^{50} erg in protons and 2.6×10^{50} erg in helium, respectively, which is compatible with the expectation that $\simeq 50$ – 60% of the explosion energy are transferred into relativistic particles in the case of efficient CR accelerators [33–35].

III. LOCAL MATTER DENSITY FROM DUST MAPS

While dust contributes only a small mass fraction to the interstellar medium (ISM), it efficiently absorbs and

¹ Data extracted from <http://snrcat.physics.umanitoba.ca/SNRtable.php>.

scatters photons with wavelengths in the visible and ultraviolet range. Therefore the distribution of dust can be used as a tracer of, e.g., gas which serves CRs as target for secondary neutrino and gamma-ray production.

Most efforts to build 3D maps of Galactic dust have been concentrated on charting dust on large scales. For instance, Ref. [36] mapped three quarters of the sky, while Ref. [37] constructed a map extending out to 3 kpc with 25 pc resolution. These maps succeeded modeling Galactic dust on large scales, but they failed to recover features on small scales because of their missing resolution. In contrast, the authors of Refs. [26, 27] concentrated their study on the closer neighborhood of the Sun, building a dust map for a $740^2 \times 540 \text{ pc}^3$ cube with a superior resolution of 1 pc. Using Gaia, 2MASS, PANSTARRS, and ALLWISE data, they deduced the G band extinction of five million stars with known parallaxes. Their results for the 3D distribution of dust are publicly available as a grid containing the e-folds of extinction per cell.

The extinction due to dust is proportional to the hydrogen column density along the grid cell as [38]

$$N_{\text{H}} = 2.87 \times 10^{21} \text{ cm}^{-2} A_{\text{V}}/\text{mag}. \quad (3)$$

Using moreover $A_{\text{G}}/A_{\text{V}} = 0.789$ as the selective extinction in the GAIA G band from Ref. [39], we obtain

$$N_{\text{H}} = 3.63 \times 10^{21} \text{ cm}^{-2} A_{\text{G}}/\text{mag}. \quad (4)$$

In addition, we account for helium which contributes 9.1% to the number density of the ISM.

In order to check the completeness of this map, we calculate the resulting average surface density Σ . Summing over the z coordinate, and multiplying by a factor 1.4 to account for helium and heavier elements, we obtain $\Sigma = 10.4 M_{\odot}/\text{pc}^2$. The comparison with the estimate $\Sigma = 13 M_{\odot}/\text{pc}^2$ for the local surface density from Ref. [40] indicates that the map includes $\simeq 80\%$ of the total gas.

Combining the obtained matter map with the CR densities and integrating along the line-of-sight, we define the function

$$\Xi^{A,A'}(E, l, b) = \int_0^{\infty} ds n_{\text{gas}}^{A'}(\mathbf{x}) I_{\text{CR}}^A(E, \mathbf{x}) \quad (5)$$

with $I_{\text{CR}}^A(E)$ as the CR intensity of nuclei with mass number A . The intensity of nuclei is in turn connected to their differential number density as $I_{\text{CR}}^A(E) = c/(4\pi)n_{\text{CR}}^A(E)$. We find in Ξ^{pp} the two prominent hot spots visible in Fig. 1: An extended region produced by CRs from the Vela SNR interacting with gas in the wall of the Local Bubble and another, smaller one produced by CRs from the SNR G074.0-08.5 in the Cygnus Loop. The latter one is close in position with the hottest spot in the IceCube neutrino data, and we will therefore discuss this possible excess first.

As shown in Fig. 1 of the Appendix, CRs emitted by the Cygnus SNR propagate along a magnetic field line

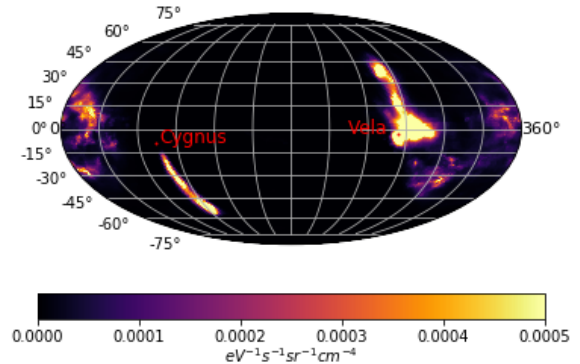


FIG. 1: The function $\Xi(E, l, b)$ in Galactic coordinates for the proton energy $E = 3 \text{ PeV}$.

away from the Galactic plane until they reach a region of increased gas density close to the boundary of the Local Bubble where the interaction probability $\propto \Xi(E, l, b)$ has a maximum. The position of the hot spot is approximately determined by the intersection of the ellipsoid filled by CRs and the boundary of the Local Bubble. From the left panel of Fig. 2, we see that the hot spot predicted by us using the Jansson-Farrar model for the GMF is around 10° – 15° offset against the most significant point in the search for point sources found by IceCube. However, rather small changes in the direction of the magnetic field line connected to the Cygnus SNR could reconcile the predicted and the observed position of the hot spot: In Fig. 3, we show the projection of the JF magnetic field line passing through Cygnus (blue line) on the Galactic plane and perpendicular to the Galactic plane, together with the position of the IceCube hot spot varying its distance as a red line. (Since the hot spot is observed on 2D, its 3D projection result in a line.) From the bottom panel of Fig. 3, we can see that the MF line passing through Cygnus crosses the hot spot line in the x - z plane. From the top panel of Fig. 3, it is clear that a rather small rotation (anti-clockwise) by $\simeq 5^\circ$ of the magnetic field line in the Galactic plane would be sufficient to align CRs from the Cygnus loop SNR with the position of the IceCube hot spot. Note also that small changes in the position of the hot spot would not lead to large changes in the resulting neutrino intensity, because the gas density in the hot spot is not atypically large, $n_{\text{gas}} \simeq 0.6/\text{cm}^3$, compared to other, close parts of the boundary of the Local Bubble.

In order to support this statement, we have also studied the resulting neutrino hot spot in another GMF model, the one of Prouza and Smida [41], where we adjusted the ratio between the turbulent to regular magnetic field in order to obey to B/C measurements. The resulting neutrino intensity is shown in the right panel of Fig. 2. One can see that the predicted hot spot in this model overlaps nicely with the observed excess in

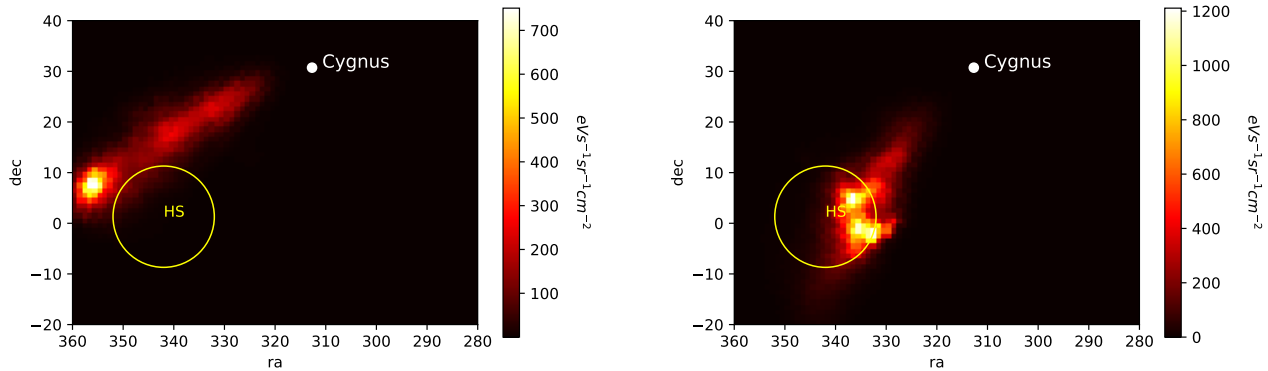


FIG. 2: Neutrino intensity $E^2 I_\nu(E, \alpha, \delta)$ in equatorial coordinates close to the hot spot for neutrino energies $E = 100$ TeV ; in the Jansson-Farrar model (left) and the Prouza-Smida model (right). The yellow circle shows the most significant region in the IceCube search for point sources.

the IceCube search for point sources.

Finally, we want to discuss the second hot spot produced by CRs from Vela which is predicted by our model. Although more prominent, the corresponding neutrino signal is, at first sight, absent in the IceCube HESE sample. In order to investigate this issue more, we show in Fig. 4 the arrival directions of the public IceCube neutrino events together with the position of Vela (black triangle) and the superbubble Loop I (orange circle). This superbubble interfaces with the Local Bubble, while the Vela SNR is close to its boundary. Both bubbles should lead to large deviations from the global regular field predicted in GMF models like the ones of Jansson-Farrar and Prouza-Smida. However, the two GMF models used by us have been only modified to account for the presence of the Local Bubble, while our calculations of CR trajectories do not take into account the effect of Loop I. If CRs would be deflected by the enhanced magnetic field in the wall of Loop I similarly as in the wall of the Local Bubble, an increase of neutrino events along the shell of Loop I close to Vela should result. As an illustration of this effect, we show in Fig. 4 the segment of Loop I close to the intersection of the magnetic field line in the Jansson-Farrar model as a hatched area. The number of HESE neutrino events in this area is ten, while six neutrinos are expected. Thus one may speculate that this excess is connected to CRs from the Vela SNR.

IV. NEUTRINO INTENSITY

We concentrate first on the neutrinos produced by CRs from SNR G074.0-08.5 in the Cygnus Loop. In this section, we report the results of our numerical calculations which we compare in the appendix with analytical estimates. Because of the rather large uncertainty in the distance to this SNR, $d = (0.5 - 1)$ kpc, we consider two cases, choosing as the distance the average ($d = 0.75$ kpc)

and the minimal value ($d = 0.5$ kpc) of this range, respectively, and choosing for the GMF the JF model. The intensity $I_\nu(E, l, b)$ of neutrinos with energy E emitted along the line-of-sight with direction (l, b) is given by

$$I_\nu(E, l, b) = \sum_{A, A'} \int_E^\infty dE' \Xi^{A, A'}(E', l, b) \frac{d\sigma^{AA' \rightarrow \nu}(E', E)}{dE}. \quad (6)$$

We include both for the target gas and the CRs the contribution of protons and helium nuclei, $A, A' = \{p, \text{He}\}$. The neutrino production cross sections are evaluated with **AAfrag** [42]. In the left panel of Fig. 2, we show the resulting neutrino intensity I_ν for the energy $E = 100$ TeV in equatorial coordinates, i.e. as function of right ascension α and declination δ for $d = 0.5$ kpc. For the larger source distance, $d = 0.75$ kpc, the hot spot in the neutrino intensity shrinks slightly in size, while its position is nearly unchanged. The maximum of $I_\nu(E, \alpha, \delta)$ corresponds to $\simeq 400$ times the isotropic neutrino intensity measured by IceCube. In the case of the larger source distance, $d = 0.75$ kpc, the neutrino intensity is reduced by one third.

We define the equivalent isotropic intensity of a specific source as

$$\langle I_\nu(E) \rangle \equiv \frac{1}{4\pi} \int d\Omega w(E) I_\nu(E, l, b) \quad (7)$$

with the weight $w(E)$ set to one. Since the observed neutrino intensity $I_\nu^{\text{obs}}(E)$ is approximately isotropic, the ratio $I_\nu(E)/I_\nu^{\text{obs}}(E)$ corresponds to the fraction of neutrino events with energy E from a given source observed by an experiment with uniform exposure. In Fig. 5, we show the isotropic neutrino intensity $\langle I_\nu(E) \rangle$ produced by CRs from the Cygnus Loop together with Ice Cube data from Ref. [43]. Note that the neutrino flux is dominated by the contribution from helium primaries which have a larger interaction probability and dominate above $E \simeq 10^{14}$ eV

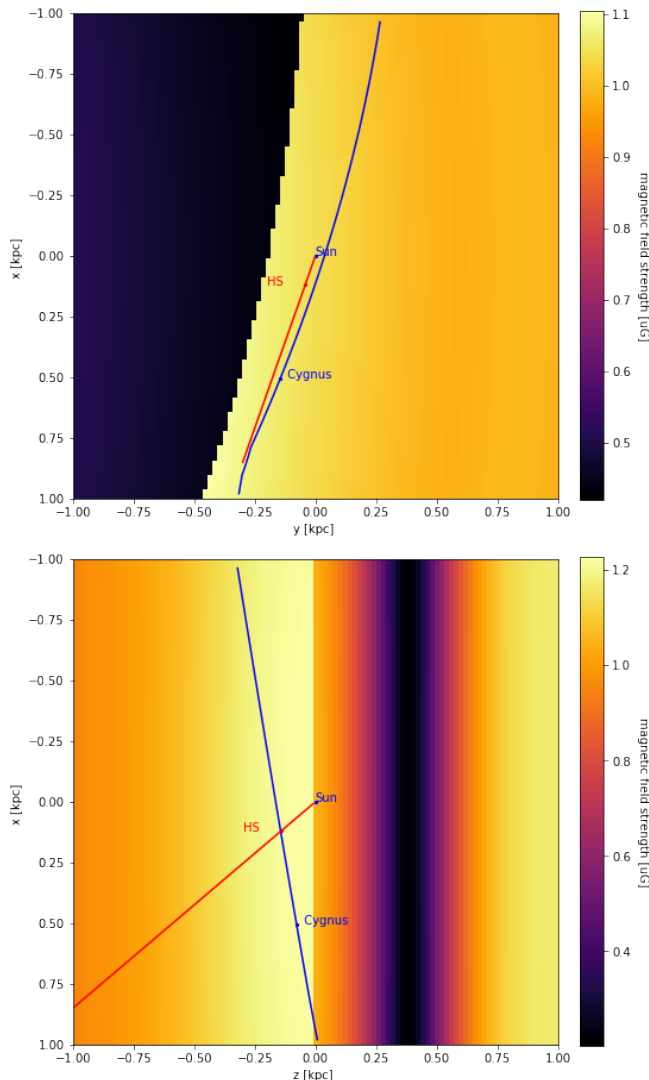


FIG. 3: The projection of the magnetic field line passing through the Cygnus loop SNR is shown in blue and the position of the Sun in black. The red line represent the position of the IceCube hot spot for varying R , the red point corresponds to the position of the IceCube hot spot for $R_{hs} = 194$ pc.

the CR injection spectrum defined in Eq. (2). Additionally, we compare the intensity of photons to the sensitivity of the LHAASO experiment estimated in Ref. [44].

For a specific experiment like IceCube, we have to account for the declination dependence of the effective area $A_{\text{eff}}(E, \delta)$. For the HESE data set, we use the effective area $A_{\text{eff}}(E)$ from Ref. [5] and deduce the declination dependence from Ref. [45], see App. B for details. Since the extension of the hot spot is small, we can neglect the declination dependence of the weight, setting $w = A_{\text{eff}}(E, \delta_s)/A_{\text{eff}}(E) \simeq 1$ with $\delta \simeq 0^\circ$ for the hot spot of IceCube.

We estimate the number of expected neutrino events

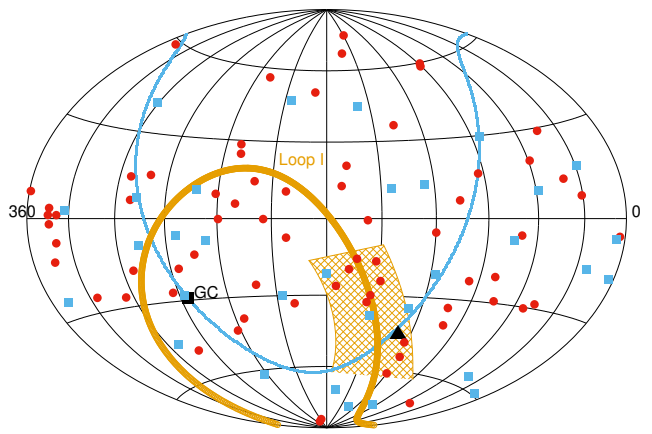


FIG. 4: HESE (red dots) and muon (blue boxes) neutrino events, Vela (black triangle), Loop I and the chosen segment (hatched area) are shown in equatorial coordinates.

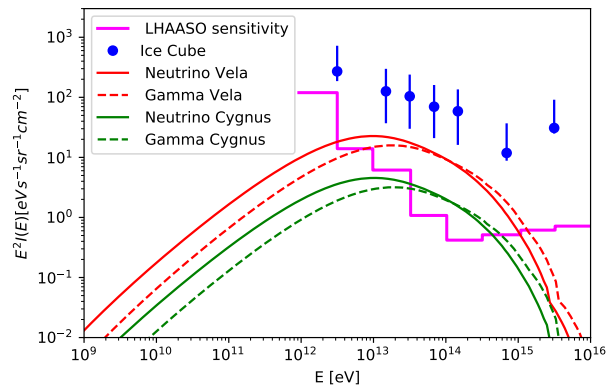


FIG. 5: Equivalent isotropic intensity of a neutrinos and photons produced by CRs from the Cygnus Loop in green and Vela in red are compared to IceCube data [43] and the estimated sensitivity of the LHAASO experiment [44].

above the minimal energy E_0 as

$$N_\nu(E > E_0) = wT \int_{E_0}^{\infty} dE \int d\Omega A_{\text{eff}}(E) I_\nu(E, l, b), \quad (8)$$

where T is the observation time. With $E_0 = 60$ TeV, we find that the hot spot produced by CRs from the Cygnus loop corresponds to two neutrino events, while four neutrino events in the HESE (event ID 44, 67, 74 with corresponding energies of 84.6 TeV, 165 TeV, 71.3 TeV respectively, and event 105) may be associated with hot spot found in the IceCube analysis. Repeating these calculations for the GMF model of Prouza and Smida, the estimated number of neutrino event increases to $\sim 3-4$.

In Fig. 5, we show additionally the isotropic neutrino intensity $\langle I_\nu(E) \rangle$ produced by CRs from Vela, using our default parameters for the injected CR power and spectra. This intensity is around a factor of six higher than

the one from the Cygnus loop using the JF model and would correspond thus to 8–16 neutrino events. Hence, the CR power injected by Vela would have to be reduced by a factor 2–3, or the CRs should be spread over a larger segment of Loop I, to be consistent with the IceCube observations.

V. DISCUSSION

First, we should comment on the fact that our model contains various uncertain parameters, leading to a corresponding spread in our predictions for the resulting secondary fluxes. We previously presented in Ref. [20] the dependence of our results varying the parameters of our magnetic field model for the Local Bubble. One should also take into account the uncertainties of the GMF model adopted: In this case, we employed two different models that gave similar results. Additional uncertainties are connected to the dust maps, that are of the order of 10%. Finally, variations in the injection spectrum, the composition and the power of individual sources may affect our results for the secondary fluxes.

In the previous sections, we have considered only SNRs with a distance from the Sun smaller than 1 kpc. Let us now verify that other SNRs similar to the Cygnus Loop but at larger distances contribute a smaller number of events to the IceCube data. There are about ten such sources in a 1 kpc region around the Sun, which corresponds to about 7000 sources in the Galaxy. The Cygnus Loop SNR contributes about 2–4 events to the IceCube data set due to the interactions of CRs with the Local Bubble at the distance of $\simeq 100$ pc. Thus the same source at 1 kpc contributes 0.02–0.04 events, bringing the contribution of nearby sources which are not connected by a magnetic field line to the Sun to 0.2–0.4 events. For sources at 10 kpc distance, the contribution of a single source is reduced to 0.0002–0.0004 events. With about 3000 of such sources, they add 0.6–1.2 events. All together, we expect about one or two events in IceCube from similar sources in the whole Galaxy, which is consistent with the limits on the contribution from the Galactic plane deduced from the IceCube data.

Next, we comment on the prospects for the detection of gamma-rays which are produced in association with neutrinos in the hot spot. Since the predicted gamma-ray emission from the hot spot is not point-like but rather extended, its detection is challenging and depends strongly on the rejection capability of hadron in the considered gamma-ray experiment. HAWC can detect a diffuse gamma-ray flux on a level comparable to the over-all diffuse neutrino flux measured by IceCube shown, but is not sensitive enough to detect the expected gamma-ray flux from the hot spot shown in Fig. 5. Limits on the gamma-ray flux at energies $E \sim 100$ TeV can also be derived from data of the ASgamma experiment [47]. For instance, in Ref. [48] a limit on the equivalent isotropic gamma-ray intensity was derived which can be compared

to flux from the hot spot presented in Fig. 5. At 400 TeV, the expected flux is around $1 \text{ eV/cm}^2/\text{s/sr}$, while the limit from ASgamma is an order of magnitude higher. At 1 PeV, the expected gamma-ray flux is $0.3 \text{ eV/cm}^2/\text{s/sr}$, while the limit from ASgamma is five times higher. In contrast, the more sensitive LHAASO experiment [46] should be able to detect the photon flux from the hot spot in the energy range $E \sim 100$ TeV, but the required time of data taking will depend on the extension of the hot spot: In the case of the JF model shown in the left panel of Fig. 1, we can estimate the gamma flux at 100 TeV as $E^2 \mathcal{F}_\gamma \simeq E^2 I_\gamma \times \Omega \simeq 7 \times 10^{-12} \text{ erg/cm}^2/\text{s}$, assuming a radius of 3° of the hot spot with an intensity of $I_\gamma \simeq 500 \text{ eV/cm}^2/\text{s/sr}$. Rescaling the sensitivity S of LHAASO for point sources, S_{point} , as $S = S_{\text{point}} \delta / \delta_{\text{PSF}}$, where $\delta_{\text{PSF}} \simeq 0.3^\circ$ is the extension of the point-spread function and δ the one of the extended source, it follows $S \simeq 4 \times 10^{-13} \text{ erg/cm}^2/\text{s}$. Although being very crude, this estimate suggests that such a concentrated hot spot should be easily detectable for LHAASO within one year of data taking. The hot spot is more difficult to detect if its extension, for the same flux, is wider, since then the CR background increases. Such a larger extension is expected in the PS model, or more generally, for a relative increase of the turbulent to the regular magnetic field. Moreover, the larger extension would be still consistent with the one of the IceCube’s hot spot.

One should not confuse the Cygnus superbubble which is located in Galactic plane [49, 50] with the Cygnus Loop SNR, considered here. In the case of sources located in the Cygnus superbubble, one expects secondary gamma-rays and neutrinos in the same region. In contrast, the neutrinos and gamma-ray emission considered here is produced after CRs streaming away from the Galactic disk hit gas clouds close to the boundary of the Local Bubble.

Finally, let us comment on the recent detection of 0.1–1 PeV diffuse gamma-rays reported by the Tibet ASgamma collaboration [47]. In their event sample, all gamma rays with energies above 398 TeV were separated by more than 0.5° from known TeV sources. In the scenario of anisotropic CR diffusion discussed here, such a separation arises rather naturally. This measurement combined with Fermi LAT data at TeV energies indicate also that the photon flux in the outer Galaxy is rather hard, $1/E^{2.5}$ [51].

VI. CONCLUSIONS

We have proposed in this work that CRs from the SNR G074.0-08.5 in the Cygnus Loop interacting with gas close to the boundary of the Local Bubble lead to an hot spot in the neutrino flux. Anisotropic diffusion of CRs is a necessary ingredient of this proposal, leading to enhanced CR densities along magnetic field lines connected to CR sources. The position of this hot spot is compatible with the most significant point in the Ice-

Cube search for point sources, and the neutrino intensity estimated by us corresponds to two to four events with energy above 60 TeV. In addition, we have proposed that CRs from the Vela SNR are spread out by the magnetic field in the boundary of the superbubble Loop I, leading to an excess of neutrino events in a segment of Loop I directed towards Vela. The corresponding photon fluxes should be detectable by LHAASO soon, providing a clear signature for a Galactic origin of the hot spot in the neutrino flux observed by IceCube.

Acknowledgments

We would like to thank Austin Schneider for comments on the IceCube exposure, and Torsten Enßlin and especially Rainer Leike for advice on the use of their extinction maps. The work of D.S. was supported in part by the Ministry of Science and Higher Education of the Russian Federation under the contract 075-15-2020-778 in the framework of the program “Large Scientific Projects” within the national project “Science”.

Appendix A: Comparison with analytical estimates

1. Cosmic ray density

For our analytical estimates, we assume that the Cygnus Loop SNR (G074.0-08.5) injected instantaneously 6×10^{50} erg in CRs, following a power law with $Q(E) = Q_0(E/E_0)^{-\alpha}$ and $\alpha \simeq 2.2$ for the injection spectrum. To be definite, we split the total energy between protons and helium nuclei as 4:3. Choosing the lowest injection energy of protons as the normalization energy, $E_0 = 1$ GeV, it follows then $Q_p = E_p/(5E_0^2) \simeq 4.3 \times 10^{52}/\text{GeV}$. Similarly, it follows $Q_{\text{He}} = 4E_{\text{He}}/(15E_0^2) \simeq Q_p$ for the normalization of the helium flux above the minimal injection energy 4 GeV.

The diffusion approximation can be applied once CRs have reached distances from the source that are greater than a few times the coherence length of the turbulent magnetic field [52, 53], which is around $L_{\text{coh}} \approx 10$ pc close to the disk. At a given energy, the functional behavior of the observed CR flux from a single source at the distance L and with the age τ can be divided into three regimes: For $2D\tau \ll L^2$, the diffuse flux is exponentially suppressed, while for intermediate times it is given by

$$I(E) \simeq \frac{c}{4\pi} \frac{Q(E)}{V(t)}. \quad (\text{A1})$$

Here, $V(t) = 4\pi L_{\perp}^2 L_{\parallel}/3$ is the volume of the ellipsoid with major axis $L_{\parallel} = (2D_{\parallel}t)^{1/2}$ and minor axis $L_{\perp} = (2D_{\perp}t)^{1/2}$. When the diffusion front reaches the edge of the Galactic CR halo, CRs start to escape and the slope of the CR intensity steepens.

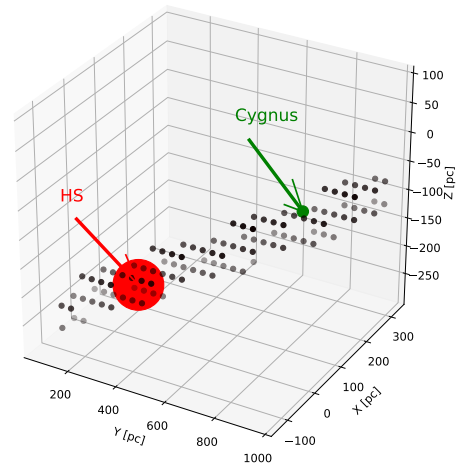


FIG. 6: Volume satisfying $I > 0.01I_{\text{max}}$ at the proton energy $E = 10^{14}$ eV together with the position of the hot spot and the Cygnus Loop SNR.

For the numerical values of the diffusion coefficients in the case of anisotropic diffusion, we read from Fig. 4 from Ref. [25] with $\eta = 0.25$ and $D_{\text{iso}} \simeq 1 \times 10^{30} \text{cm}^2/\text{s}$ valid at the reference energy $E_* = 10^{14}$ eV that $D_{\parallel} \simeq 5D_{\text{iso}}$, while $D_{\perp} \simeq D_{\text{iso}}/500$. Hence CRs with energy E_* fill an ellipsoid with major axis $L_{\parallel} \simeq 700$ pc and minor axis $L_{\perp} \simeq 14$ pc. The CR intensity of protons inside this ellipsoid can be estimated with $V \simeq 1.7 \times 10^{61} \text{cm}^3$ as $E_* I(E_*) \simeq 6 \times 10^{-6}/(\text{cm}^2 \text{sr})$.

In Fig. 6, we show for comparison the cells satisfying the condition $I(E) > 0.01I_{\text{max}}(E)$ at $E = 10^{14}$ eV in our numerical simulations together with the position of the hot spot and of the Cygnus Loop SNR. One can see that the CRs fill a tube with diameter 50 pc, what agrees quite well with the expectation $\sim 6 \times 2D_{\perp}\tau \simeq 80$ pc for $I(E) = 0.01I_{\text{max}}(E)$. Moreover, the distance between the hot spot and the Cygnus Loop SNR is around 530 pc and the CR tube extends until it touches the Local Bubble. Note also this diameter is much larger than the extension of a SNR at the age of few hundred years; thus our assumption of a point-like injection is justified.

2. Neutrino production

In order to obtain an estimate for the equivalent isotropic neutrino intensity, we define first the volume \mathcal{V} of the neutrino emitting region by the condition

$$n_{\text{gas}}(\mathbf{x}) I_{\text{CR}}(E_*, \mathbf{x}) > 0.01 \max_{\mathbf{x} \in \text{box}} \{n_{\text{gas}}(\mathbf{x}) I_{\text{CR}}(E_*, \mathbf{x})\} \quad (\text{A2})$$

at a given energy E_* . Then we introduce in²

$$I_\nu(E) = \frac{c}{4\pi} \sum_{A,A' \in \{1,4\}} \int_E^\infty dE' \frac{d\sigma_{\text{inel}}^{AA' \rightarrow \nu}(E', E)}{dE} \quad (\text{A3})$$

$$\times \int d^3x \frac{n_A(E', \mathbf{x}) n_{\text{gas}}^{A'}(\mathbf{x})}{4\pi d^2},$$

the inelastic cross section $\sigma_{\text{inel}}^{AA'}$, the spectrally averaged energy fraction $\langle y^{\alpha-1} \rangle$ transferred to neutrinos, and the total number of gas particles $N_{\text{gas}} = \sum_A \int_V d^3x n_{\text{gas}}^A(\mathbf{x})$ in the source region \mathcal{V} . Moreover, we neglect the extension of the source region, obtaining

$$I_\nu(E) \simeq \sum_{A,A'} \frac{f_{A'} N_{\text{gas}}}{4\pi d^2} \langle y^{\alpha-1} \rangle \sigma_{\text{inel}}^{AA' \rightarrow \nu}(E) \langle I_A(E) \rangle, \quad (\text{A4})$$

where d denotes the distance to the source volume \mathcal{V} , f_A the fraction of proton and helium nuclei in the gas, and $\langle I_A(E') \rangle$ the spatially averaged intensity of CR protons and helium nuclei.

At the energy $E_* = 10^{14}$ eV, the condition (A2) is satisfied in 750 cells of size $(6 \text{ pc})^3$, resulting with $\langle n_{\text{gas}} \rangle \simeq 0.56/\text{cm}^3$ into $N_{\text{gas}} \simeq 2 \times 10^{60}$. The intensity of CR protons obtained from our numerical simulations and averaged over this volume is $\langle E_* I_p(E_*) \rangle \simeq 4 \times 10^{-6}/\text{cm}^2/\text{s}/\text{sr}$, i.e. agrees well with our estimate using the diffusion approximation in the previous subsection.

With $d \simeq 270 \text{ pc}$ and $Z(E_*, \alpha) = \langle y^{\alpha-1} \rangle \sigma_{\text{inel}}^{pp} \simeq 7 \text{ mbarn}$ for the Z factor for the production of neutrinos from a power law with $\alpha \simeq 2.2$, this leads to

$$E_*^2 I_\nu^{pp}(E_*) \simeq 1.0 \frac{\text{eV}}{\text{cm}^2 \text{ s sr}}$$

for the isotropic neutrino intensity due to pp interactions. We can estimate the contribution of helium projectiles and targets at energies $E_\nu \lesssim 10^{13}$ eV setting $I_p(E) \simeq I_{\text{He}}(E)$ valid for primary energies $\lesssim 10^{14}$ eV. With $\sigma_{\text{inel}}^{pp} \simeq 48 \text{ mbarn}$, $\sigma_{\text{inel}}^{p\text{He}} \simeq 148 \text{ mbarn}$, $\sigma_{\text{inel}}^{\text{He}p} \simeq 137 \text{ mbarn}$ and $\sigma_{\text{inel}}^{\text{HeHe}} \simeq 324 \text{ mbarn}$, it follows then

$$\frac{I_\nu^{\text{tot}}}{I_\nu^{pp}} \simeq \frac{0.9(\sigma_{\text{inel}}^{pp} + \sigma_{\text{inel}}^{\text{He}p}) + 0.1(\sigma_{\text{inel}}^{\text{He}p} + \sigma_{\text{inel}}^{\text{HeHe}})}{\sigma_{pp}} \simeq 4. \quad (\text{A5})$$

Thus our estimate agrees again well the numerical value shown in Fig. 5.

Appendix B: Exposure

We subtract in the Supplemental Fig. 5 of Ref. [5] the line signal+background from the background to obtain the signal $S(\delta)$ as function of the declination δ . Then we calculate with $x = \sin \delta$

$$S_{\text{av}} = \frac{1}{2} \int_{-1}^1 dx S(\delta). \quad (\text{B1})$$

The weight w of a source with declination δ follows then as $w = S(\delta)/S_{\text{av}}$.

-
- [1] G. G. Raffelt, Ann. Rev. Nucl. Part. Sci. **49**, 163 (1999), hep-ph/9903472.
- [2] T. K. Gaisser, F. Halzen, and T. Stanev, Phys. Rept. **258**, 173 (1995), [Erratum: Phys. Rept.271,355(1996)], hep-ph/9410384.
- [3] M. Kachelrieß and D. V. Semikoz, Prog. Part. Nucl. Phys. **109**, 103710 (2019), 1904.08160.
- [4] M. G. Aartsen et al. (IceCube), Astrophys. J. **833**, 3 (2016), 1607.08006.
- [5] R. Abbasi et al. (IceCube) (2020), 2011.03545.
- [6] V. Berezhinsky, A. Gazizov, M. Kachelrieß, and S. Ostapchenko, Phys. Lett. **B695**, 13 (2011), 1003.1496.
- [7] K. Murase, M. Ahlers, and B. C. Lacki, Phys. Rev. **D88**, 121301 (2013), 1306.3417.
- [8] V. S. Berezhinsky and A. Yu. Smirnov, Astrophys. Space Sci. **32**, 461 (1975).
- [9] V. S. Berezhinsky, T. K. Gaisser, F. Halzen, and T. Stanev, Astropart. Phys. **1**, 281 (1993).
- [10] M. Kachelrieß and S. Ostapchenko, Phys. Rev. **D90**, 083002 (2014), 1405.3797.
- [11] D. Gaggero, D. Grasso, A. Marinelli, A. Urbano, and M. Valli, Astrophys. J. **815**, L25 (2015), 1504.00227.
- [12] A. M. Taylor, S. Gabici, and F. Aharonian, Phys. Rev. **D89**, 103003 (2014), 1403.3206.
- [13] P. Blasi and E. Amato, Phys. Rev. Lett. **122**, 051101 (2019), 1901.03609.
- [14] V. Berezhinsky, M. Kachelrieß, and A. Vilenkin, Phys. Rev. Lett. **79**, 4302 (1997), astro-ph/9708217.
- [15] B. Feldstein, A. Kusenko, S. Matsumoto, and T. T. Yanagida, Phys. Rev. **D88**, 015004 (2013), 1303.7320.
- [16] A. Esmaili and P. D. Serpico, JCAP **1311**, 054 (2013), 1308.1105.
- [17] R. M. Crocker and F. Aharonian, Phys. Rev. Lett. **106**, 101102 (2011), 1008.2658.
- [18] C. Lunardini and S. Razzaque, Phys. Rev. Lett. **108**, 221102 (2012), 1112.4799.
- [19] K. J. Andersen, M. Kachelrieß, and D. V. Semikoz, Astrophys. J. **861**, L19 (2018), 1712.03153.
- [20] M. Bouyahiaoui, M. Kachelrieß, and D. V. Semikoz, Phys. Rev. D **101**, 123023 (2020), 2001.00768.
- [21] F. L. Villante and F. Vissani, Phys. Rev. D **78**, 103007 (2008), 0807.4151.
- [22] M. Bouyahiaoui, M. Kachelrieß, and D. Semikoz, PoS **ICRC2021**, 999 (2021), 2105.13378.
- [23] G. Giacinti, M. Kachelrieß, and D. V. Semikoz, Phys. Rev. **D90**, 041302 (2014), 1403.3380.

- [24] G. Giacinti, M. Kachelrieß, and D. V. Semikoz, *Phys. Rev.* **D91**, 083009 (2015), 1502.01608.
- [25] G. Giacinti, M. Kachelrieß, and D. V. Semikoz, *JCAP* **1807**, 051 (2018), 1710.08205.
- [26] R. H. Leike and T. A. Enßlin, *Astron. Astrophys.* **631**, A32 (2019).
- [27] R. H. Leike, M. Glatzle, and T. A. Enßlin, *Astron. Astrophys.* **639**, A138 (2020).
- [28] M. Bouyahiaoui, M. Kachelrieß, and D. V. Semikoz, *JCAP* **1901**, 046 (2019), 1812.03522.
- [29] R. Jansson and G. R. Farrar, *Astrophys.J.* **761**, L11 (2012), 1210.7820.
- [30] R. Jansson and G. R. Farrar, *Astrophys.J.* **757**, 14 (2012), 1204.3662.
- [31] G. Giacinti, M. Kachelrieß, D. V. Semikoz, and G. Sigl, *JCAP* **1207**, 031 (2012), 1112.5599.
- [32] G. Giacinti, M. Kachelrieß, D. V. Semikoz, and G. Sigl, *Astropart. Phys.* **35**, 192 (2011), 1104.1141.
- [33] A. R. Bell and S. G. Lucek, *Mon. Not. Roy. Astron. Soc.* **321**, 433 (2001).
- [34] D. C. Ellison, A. Decourchelle, and J. Ballet, *Astron. Astrophys.* **413**, 189 (2004), astro-ph/0308308.
- [35] A. R. Bell, *Mon. Not. Roy. Astron. Soc.* **353**, 550 (2004).
- [36] G. M. Green, E. Schlafly, C. Zucker, J. S. Speagle, and D. Finkbeiner, *Astrophys. J.* **887**, 93 (2019), 1905.02734.
- [37] R. Lallement, L. Capitano, L. Ruiz-Dern, C. Danielski, C. Babusiaux, L. Vergely, M. Elyajouri, F. Arenou, and N. Leclerc, *Astron. Astrophys.* **616**, A132 (2018).
- [38] D. R. Foight, T. Güver, F. Özel, and P. O. Slane, *Astrophys. J.* **826**, 66 (2016), 1504.07274.
- [39] S. Wang and X. Chen, *Astrophys. J.* **877**, 116 (2019), 1904.04575.
- [40] C. Flynn, J. Holmberg, L. Portinari, B. Fuchs, and H. Jahreiss, *Mon. Not. Roy. Astron. Soc.* **372**, 1149 (2006), astro-ph/0608193.
- [41] M. Prouza and R. Smida, *Astron. Astrophys.* **410**, 1 (2003), astro-ph/0307165.
- [42] M. Kachelrieß, I. V. Moskalenko, and S. Ostapchenko, *Comput. Phys. Commun.* **245**, 106846 (2019), 1904.05129.
- [43] M. G. Aartsen et al. (IceCube), *Astrophys. J.* **849**, 67 (2017), 1707.03416.
- [44] A. Neronov and D. Semikoz, *Phys. Rev. D* **102**, 043025 (2020), 2001.11881.
- [45] M. G. Aartsen et al. (IceCube), *Phys. Rev. Lett.* **113**, 101101 (2014), 1405.5303.
- [46] A. Addazi et al., *Chin. Phys. C* **46**, 035001 (2022), 1905.02773.
- [47] M. Amenomori et al. (Tibet ASgamma), *Phys. Rev. Lett.* **126**, 141101 (2021), 2104.05181.
- [48] A. Neronov, D. Semikoz, and I. Vovk, *Astron. Astrophys.* **653**, L4 (2021), 2107.06541.
- [49] A. U. Abeysekara et al. (2021), 2103.06820.
- [50] D. D. Dzhappuev et al. (2021), 2105.07242.
- [51] S. Koldobskiy, A. Neronov, and D. Semikoz (2021), 2105.00959.
- [52] G. Giacinti, M. Kachelrieß, and D. V. Semikoz, *Phys. Rev. Lett.* **108**, 261101 (2012), 1204.1271.
- [53] G. Giacinti, M. Kachelrieß, and D. V. Semikoz, *Phys. Rev.* **D88**, 023010 (2013), 1306.3209.